Molecular Medicine

Modulation of Poly(ADP-Ribose) Polymerase-1 (PARP-1)-Mediated Oxidative Cell Injury by Ring Finger Protein 146 (RNF146) in Cardiac Myocytes

Domokos Gerö,[1] Petra Szoleczky,[1] Athanasia Chatzianastasiou,[2] Andreas Papapetropoulos,[2] and Csaba Szabo[1]

[1]Department of Anesthesiology, University of Texas Medical Branch, Galveston, Texas, United States of America; and [2]Faculty of Pharmacy, University of Athens, Athens, Greece

Poly(ADP-ribose) polymerase-1 (PARP-1) activation is a hallmark of oxidative stress–induced cellular injury that can lead to energetic failure and necrotic cell death via depleting the cellular nicotinamide adenine dinucleotide (NAD^+) and ATP pools. Pharmacological PARP-1 inhibition or genetic PARP-1 deficiency exert protective effects in multiple models of cardiomyocyte injury. However, the connection between nuclear PARP-1 activation and depletion of the cytoplasmic and mitochondrial energy pools is poorly understood. By using cultured rat cardiomyocytes, here we report that ring finger protein 146 (RNF146), a cytoplasmic E3-ubiquitin ligase, acts as a direct interactor of PARP-1. Overexpression of RNF146 exerts protection against oxidant-induced cell death, whereas PARP-1–mediated cellular injury is augmented after RNF146 silencing. RNF146 translocates to the nucleus upon PARP-1 activation, triggering the exit of PARP-1 from the nucleus, followed by rapid degradation of both proteins. PARP-1 and RNF146 degradation occurs in the early phase of myocardial ischemia-reperfusion injury; it precedes the induction of heat shock protein expression. Taken together, PARP-1 release from the nucleus and its rapid degradation represent newly identified steps of the necrotic cell death program induced by oxidative stress. These steps are controlled by the ubiquitin-proteasome pathway protein RNF146. The current results shed new light on the mechanism of necrotic cell death. RNF146 may represent a distinct target for experimental therapeutic intervention of oxidant-mediated cardiac injury.

Online address: http://www.molmed.org
doi: 10.2119/molmed.2014.00102

INTRODUCTION

Poly(ADP-ribose) polymerase-1 (PARP-1) is a ubiquitously expressed enzyme that catalyzes the poly(ADP-ribosyl)ation of acceptor proteins by using nicotinamide adenine dinucleotide (NAD^+) as a substrate. The protein consists of an N-terminal DNA-binding domain, an automodification domain and a C-terminal catalytic domain. PARP-1 has low basal enzymatic activity, but its catalytic activity is dramatically stimulated on binding to damaged DNA (single or double strand breaks). Targets of the enzyme include histone proteins and transcription-related factors and PARP-1 itself (via its automodification domain). PARylation can affect the target protein function and its interactions with various proteins and DNA; thereby, PARP-1 plays a key role in the regulation of DNA repair and gene transcription (1,2).

Traditionally, the regulation of nuclear DNA repair and maintenance of genomic integrity was considered the main physiological function of PARP-1. The functional roles of PARP-1 were later extended by the discovery that PARP-1 acts as a coactivator and corepressor of gene transcription, thereby regulating the production of inflammatory mediators (1,2). In response to massive amount of DNA damage, PARP-1 can become so robustly activated that it can lead to a marked depletion of the cellular pool of its substrate (NAD^+), culminating in a catastrophic cellular energetic deficit (1,2). Overactivation of PARP-1 has been implicated in a variety of pathophysiological conditions, including ischemia-reperfusion injury, critical illness, pancreatic β-cell injury, diabetic complications and neurodegeneration (1,2). It also plays a role in the pathogenesis of myocardial ischemia reperfusion, where PARP-1 genetic deficiency and pharmacological PARP inhibition exert cardioprotective effects (1–6).

Energetic failure following PARP-1 activation is not only a result of direct NAD^+ consumption, but it is also trig-

Address correspondence to *Csaba Szabo, Department of Anesthesiology, University of Texas Medical Branch, 610 Harboside Drive, Bldg. 21, Room 4.202H, Galveston, TX 77555-1102. Phone: 409-747-5384; Fax: 409-747-5384; E-mail: szabocsaba@aol.com.*
Submitted May 9, 2014; Accepted for publication May 13, 2014; Epub (www.molmed.org) ahead of print May 14, 2014.

gered by mitochondrial dysfunction induced by negatively charged poly(ADP-ribose) (PAR) polymers, which are the principal products of PARP-1 and can be subsequently "liberated" from the PARylated proteins by various enzymes including PAR glycohydrolase (7,8). In the early phase of oxidative injury, enzymatic NAD^+ consumption appears to be more important, and cell death mostly occurs via necrosis. However, in the late phase of the injury, diminished mitochondrial output and release of pro-apoptotic molecules from the mitochondria play a dominant role, leading to various forms of programmed cell death (including apoptosis and parthanathos).

Recent work, using differential display to identify genes induced in the late phase of oxidant injury, led to the discovery of the PAR-interacting protein RNF146. Transgenic RNF146 exerted protection against *N*-methyl-D-aspartate (NMDA)-induced neural cell death by directly binding to the PAR polymer (9,10). Currently, all available information on the role of RNF146 in the modulation of cell death relates to neuronal injury, although the protein is expressed at high levels in most peripheral tissues. Because our pilot studies showed that RNF146 expression is the highest in the heart and muscle, the goal of the current project was to characterize the role of RNF146 in PARP-1–mediated cell death during oxidative myocyte injury *in vitro* and during myocardial ischemia-reperfusion injury *in vivo.*

MATERIALS AND METHODS

Cell Culture

H9c2 rat cardiomyocytes were purchased from American Type Culture Collection (ATCC, Manassas, VA, USA) and maintained in Dulbecco's modified Eagle medium (DMEM) (Biochrom, Berlin, Germany) supplemented with 4 mmol/L glutamine, 10% fetal bovine serum (FBS) (PAA Laboratories, Westborough, MA, USA), 100 IU/mL penicillin and 100 μg/mL streptomycin (Invitrogen/Life Technologies, Carlsbad, CA, USA) at 37°C in 10% CO_2 atmosphere.

RNF146 Silencing

H9c2 cardiomyoblasts (10,000/well) were plated on 96-well plates; the following day, the cells were transfected with *RNF146* siRNA (1 pmol/well; Silencer Select; assay ID: s158554; Life Technologies) by using Lipofectamine 2000 transfection reagent. Control cells were transfected with Silencer Select negative control #1 siRNA (ID: 4390844; Life Technologies). The knockdown efficiency was evaluated by real-time polymerase chain reaction (PCR) (Taqman assay ID: Rn02534308 using TaqMan Rodent GAPDH Control Reagents [catalog no. 4308313] normalization; Applied Biosystems/Life Technologies) and by Western blotting 48 h after transfection. The cells were exposed to oxidant injury 48 h after transfection.

RNF146 Overexpression

The complete rat RNF146 cDNA (IMAGE: 7135728; NCBI accession number BC083675) was obtained in pEXPRESS-1 vector from Life Technologies. The coding sequence was excised with *Eco*RI/*Xho*I digestion and subcloned into pcDNA3.1(+) (Life Technologies) to create the vector pcDNA-RNF146. H9c2 cells were transfected with pcDNA-RNF146 and selected with G418 (500 μg/mL; Invitrogen/Life Technologies) for 4 wks. Individual colonies were picked up and tested for RNF146 overexpression by Western blotting. RNF146 overexpressing clones were expanded, and the presence of the integrated expression cassette was confirmed by PCR. Control clones were generated by transfection of H9c2 cells with β-galactosidase expression vector [pcDNA3.1(+)/myc-His/LacZ; Invitrogen/Life Technologies] and 4-wk-long selection with G418.

Confirmation of Stable Transfection by PCRs

H9c2 cells were transfected with pcDNA-RNF146 and selected with G418 (500 μg/mL, Invitrogen) for 4 wks. Individual colonies were picked up and tested for RNF146 overexpression by Western blotting. RNF146 overexpressing clones were expanded in T75 flasks and used for DNA isolation as described (11). Cells transfected with pcDNA3.1(+)/myc-His/LacZ were selected with G418 and used as controls. Cells were pelleted by centrifuging at 200*g* for 10 min and lysed in 450 μL DNA lysis buffer (100 mmol/L Tris, pH 8.0, 20 mmol/L ethylenediaminetetraacetic acid [EDTA], 0.8% *N*-lauroylsarcosine). A total of 175 units RNase A (25 μL; 5PRIME, Gaithersburg, MD, USA) was added, and the samples were incubated at 37°C for 1 h; then 60 mAU Proteinase K (100 μL; 5PRIME) was added and incubated at 55°C overnight. DNA was isolated by subsequent phenol-chloroform extraction and ethanol precipitation. A total of 20 ng DNA was used as template in PCRs by using F1 (5′-CGTGTACGGT GGGAGGTCTA-3′) and R1 (5′-CAGGT CTCACTCGCCTTCTT-3′), F2 (5′-CGTGT ACGGTGGGAGGTCTA-3′) and R2 (5′-ATGAAGCGCCCTTTACACAC-3′) or F3 (5′-TAGTGTGTCCCCGTGCATTA-3′) and R3 (5′-GCGATGCAATTTCCTCATTT-3′) primers by using a touchdown PCR protocol. The DNA quality was checked by using PCR primers to amplify an ~1.2-kb region of the adiponectin 1 (*ADIPOR1*) gene (ADIPOR1 forward 5′-CGCATCCACACAGAAACTG-3′, ADIPOR1 reverse 5′-TGAGCATGGT CAAGATTCCC-3′).

RNF146 expression was also measured at the mRNA level. Total RNA was isolated from RNF146 overexpressing cells and pcDNA3.1(+)/myc-His/LacZ transfected controls by TRizol reagent (Invitrogen/Life Technologies). A total of 2 μg RNA was treated with DNase (Epicentre), and reverse transcription was carried out by using a High Capacity cDNA Archive kit (Applied Biosystems/Life Technologies) following the manufacturer's instructions. *RNF146* overexpression was confirmed by *RNF146* real-time PCR (Taqman assay ID: Rn02534308 using TaqMan Rodent GAPDH Control Reagents [catalog no. 4308313] normalization) and by an exon-spanning assay (RNF146 forward primer: 5′-GTGCC TGTGGGATCTGTGAT-3′, RNF146 re-

verse primer: 5′-CAGGTCTCACTCGCC TTCTT-3′ and FAM/TAMRA labeled RNF146 probe: 5′-GGCTGTGGTGAAATT GATCACTCAC-3′).

Transient Transfection of 293T Cells with the RNF146 Expression Vector

The 293T cells were purchased from American Type Culture Collection (ATCC) and maintained in DMEM supplemented with 2 mmol/L glutamine, 10% FBS (Invitrogen/Life Technologies), 100 IU/mL penicillin and 100 μg/mL streptomycin (Invitrogen/Life Technologies) at 37°C in 10% CO_2 atmosphere.

Cells were transiently transfected with pcDNA-RNF146 by a linear polyethyleneimine-based transfection reagent (ExGen500, Fermentas, Vilnius, Lithuania). Cells were exposed to H_2O_2 to induce PARP-1 activation and cell death, and viability was measured by the 3-(4,5-dimethyl-2-thiazolyl)-2,5-diphenyl-2H-tetrazolium bromide (MTT) assay after 3 h. In addition, PARP-1 activation was confirmed by Western blotting (as described below) by using an antibody against PAR at 5 min after H_2O_2.

Oxidative Stress–Induced Injury and Viability Assays

H9c2 cells (10,000/well) were plated on 96-well plates, and 48 h later, they were exposed to H_2O_2 in fresh culture medium for 3 h. Cell viability was measured by the MTT and LDH assays as described (12). (Cells exposed to siRNAs were subjected to H_2O_2 injury 48 h after transfection.) The PARP inhibitor PJ34 (3 μmol/L; Sigma-Aldrich, St. Louis, MO, USA) was added to the cells simultaneously with H_2O_2. Cell culture supernatant (30 μL) was saved for assaying the lactate dehydrogenase (LDH) release, and MTT was added to the cells at a final concentration of 0.5 mg/mL for 1 h. The converted formazan dye was dissolved in isopropanol and measured photometrically on a Synergy Mx plate reader (BioTek, Winooski, VT, USA). Viability was calculated by using a calibration curve created by measuring the MTT converting capacity of serial dilutions of H9c2 cells.

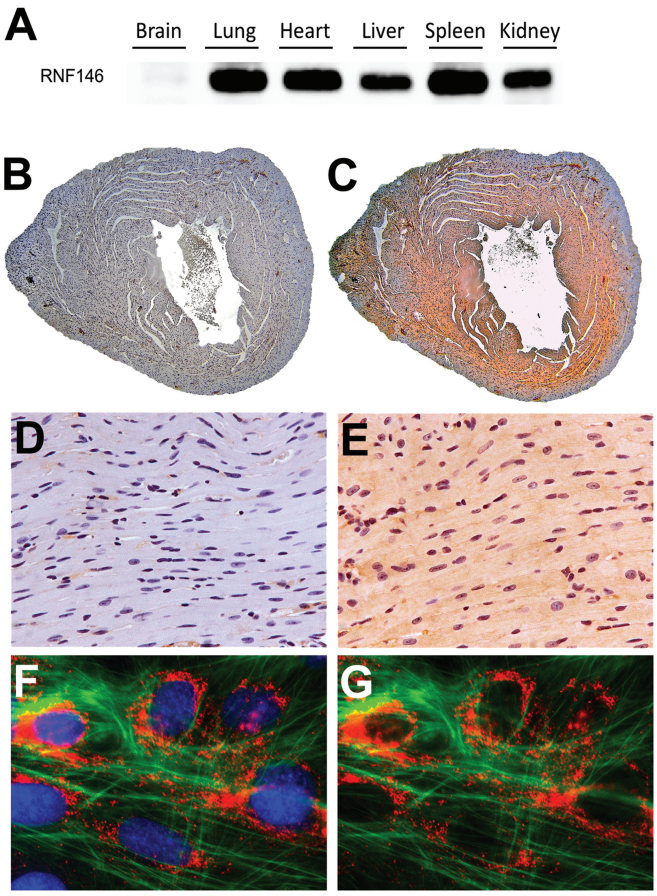

Figure 1. RNF146 expression in the heart. (A) RNF146 expression was explored by Western blotting in mouse tissues (8-wk-old male). High level of RNF146 was detected in the heart. (B–E) Immunohistochemical localization of RNF146 in the heart. Formalin-fixed paraffin-embedded heart sections were stained with anti-RNF146 antibody (C, E) or with the omission of primary antibody (B, D) and counterstained with hematoxylin. Cross-sections of the ventricles close to the apex of the heart (B, C) and higher magnification images of the myocardium show homogenous myocardial staining (D, E). (F, G) RNF146 expression was detected in the cytoplasm in H9c2 cardiomyocytes with Alexa Fluor 546 fluorescent label. (F) RNF146 staining is shown with Alexa Fluor 488 phalloidin and Hoechst 33342 nuclear counterstaining. (G) RNF146 and phalloidin channels are merged to highlight the extranuclear localization of RNF146.

LDH activity was measured by mixing the supernatant with freshly prepared LDH assay reagent [85 mmol/L lactic acid, 1,040 mmol/L NAD^+, 224 mmol/L *N*-methylphenazonium methyl sulfate, 528 mmol/L 2-(4-iodophenyl)-3-(4-nitrophenyl)-5-phenyl-2H-tetrazolium chloride, 200 mmol/L Tris, pH 8.2]. The changes in absorbance at 492 nm were measured kinetically for 15 min, and LDH activity in the supernatant is shown as the V_{max} value.

Oxygen-Glucose Deprivation Injury

Oxygen-glucose deprivation (OGD) injury was conducted as previously described (13,14). RNF146 overexpressing and control H9c2 cells (10,000/well) were plated on 96-well plates and cultured for 4 d. Culture medium was replaced with DMEM containing no glucose before the induction of hypoxia. Culture plates were

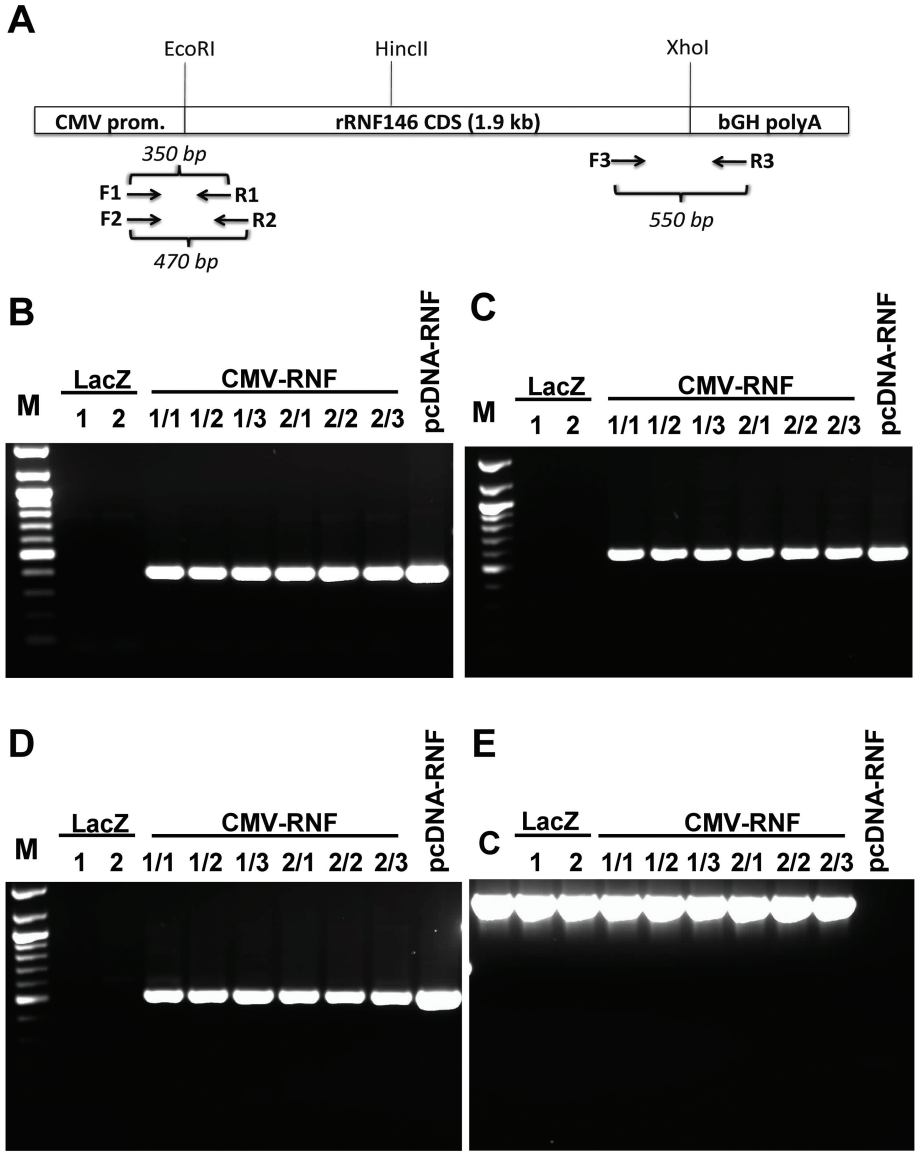

Figure 2. *RNF146* expression cassette in stable transfected clones. (A) The rat *RNF146* coding sequence (*rRNF146* CDS) was subcloned into pcDNA3.1+ vector by using *EcoR*I and *Xho*I restriction sites, and the resulting pcDNA-RNF146 vector was confirmed by using *Hinc*II digestion. H9c2 cells were stably transfected with pcDNA-RNF146, and the integration of the complete expression cassette was confirmed with the labeled PCRs. The forward (F) and reverse (R) primers are shown at their annealing positions with the size of the amplicons. (B–E) DNA was isolated from pcDNA-RNF146 stable transfected colonies (CMV-RNF) and control β-galactosidase–expressing clones (*LacZ*). The presence of the CMV-RNF146 expression cassette was confirmed with PCR. The pcDNA-RNF146 vector (pcDNA-RNF) or rat genomic DNA (C) was used as a template in control reactions. (B) Gel electrophoresis image of PCR products by using F1 and R1 primers (350–base pair (bp) PCR product) and DNA marker (M). (C) Gel electrophoresis image of PCR products using F2 and R2 primers (470-bp PCR product) to confirm the 5′ end. (D) Gel electrophoresis image of PCR products using F3 and R3 primers (550-bp PCR product) to confirm the 3′ end of the cassette. (E) Gel electrophoresis image of PCR products using adiponectin 1 PCR primers to control the DNA quality (1,200-bp PCR product).

placed in gas-tight incubation chambers (Billups-Rothenberg, Del Mar, CA, USA), and the chamber atmosphere was replaced by flushing the chamber with 95% N_2/5% CO_2 mixture at 30 L/min flow rate for 10 min. The hypoxia was maintained by clamping and incubating the chambers for 8 h at 37°C. All assay plates were subjected to hypoxia-included wells exposed to glucose-free medium (OGD) and medium containing 4.5 g/L glucose (hypoxia CTL). Cells were also exposed to glucose-free medium or maintained in glucose-containing medium (4.5 g/L glucose) under normoxia (normoxia CTL). After 8 h, glucose and serum concentration was restored by supplementing the culture medium with glucose and FBS, and the cells were incubated for 16 h at 37°C at 5% CO_2 atmosphere. MTT converting capacity ("viability") of the cells, ATP content and LDH release was measured after 8 h of hypoxia/normoxia and after the 16-h recovery period.

ATP concentration was determined by the commercially available CellTiter-Glo® Luminescent Cell Viability Assay (Promega, Madison, WI, USA). The cells were lysed in 100 μL CellTiter-Glo reagent according to the manufacturer's recommendations, and the luminescent signal was recorded for 1 s on a high-sensitivity luminometer (Synergy 2; Biotek, Winooski, VT, USA). The assay is based on ATP requiring luciferin-oxyluciferin conversion mediated by a thermostable luciferase that generates a stable "glow-type" luminescent signal.

Western Blotting

Cells were lysed in denaturing loading buffer (20 mmol/L Tris, 2% SDS, 10% glycerol, 6 mol/L urea, 100 μg/mL bromophenol blue, 200 mmol/L β-mercaptoethanol), and mouse tissue samples were homogenized in radioimmunoprecipitation assay buffer (150 mmol/L NaCl, 1% NP40, 0.5% sodium deoxycholate, 0.1% sodium dodecyl sulfate, 50 mmol/L Tris, pH 8.0) supplemented with protease inhibitors (Complete Mini EDTA-free; Roche, Indianapolis, IN, USA). Lysates were sonicated,

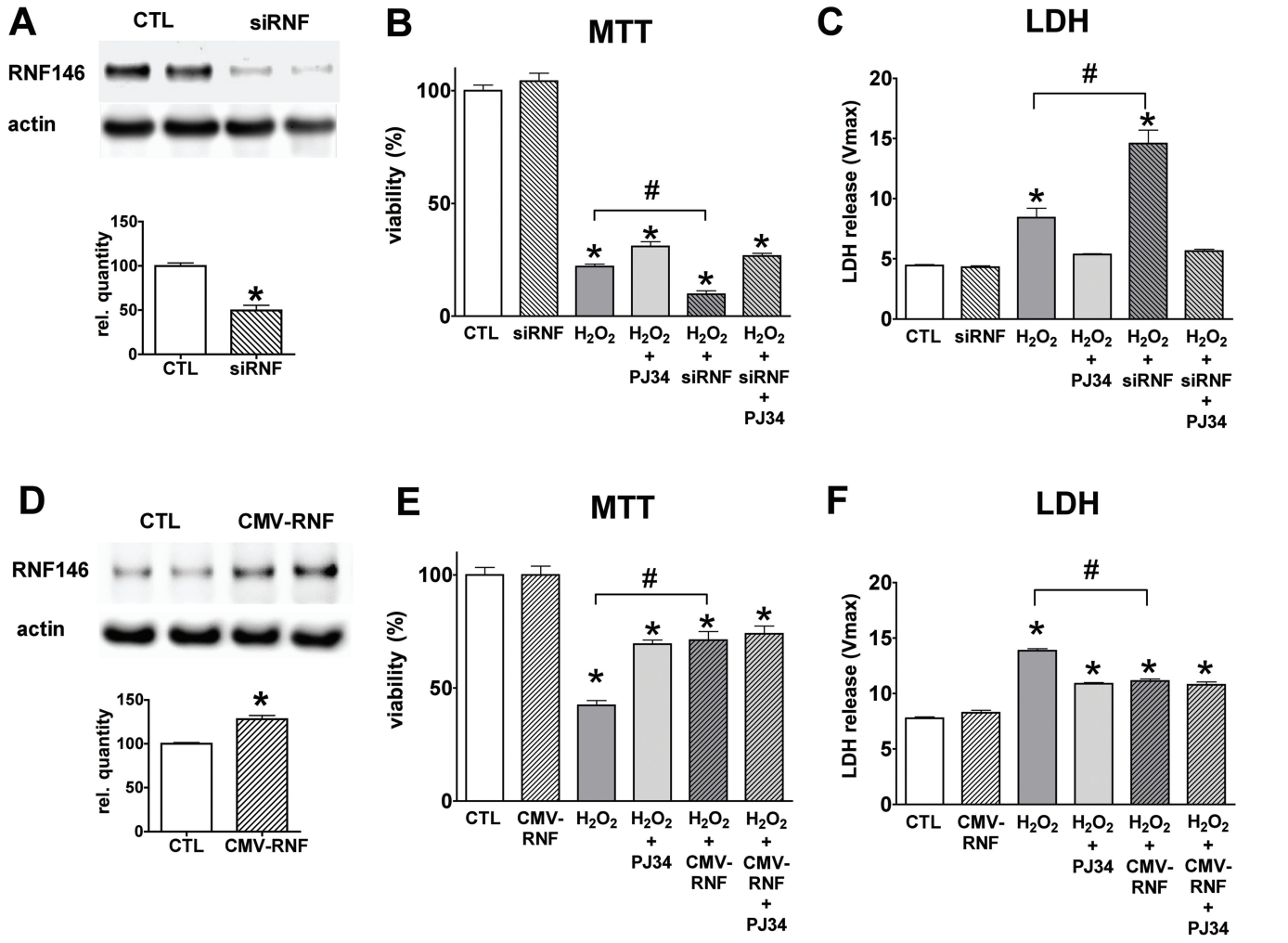

Figure 3. RNF146 controls cell death during oxidative stress. (A–C) RNF146 silencing decreases cell survival in oxidant injury. H9c2 cardiomyoblasts were transfected with RNF146 (siRNF) or negative control siRNA (CTL). (A) The knockdown efficiency was evaluated by Western blotting 48 h after transfection. (B, C) The sensitivity to H_2O_2 (600 μmol/L, 3 h) was tested with or without PARP inhibition (PJ34, 3 μmol/L). Cell viability was measured by the MTT assay (B) and LDH release was measured in the supernatant (C). (D–F) RNF146 overexpression increases cell survival during oxidative stress. (D) Overexpression of RNF146 is detectable by Western blotting in stable transfected H9c2 cells (CMV-RNF). (E, F) Oxidative stress tolerance was tested by H_2O_2 treatment in RNF146 overexpressing clones and respective controls (H9c2 cells transfected with control vector and selected with G418, CTL). Cell survival was measured by the MTT viability (E) and LDH assays (F). $^*p < 0.05$ compared with CTL; $^\#p < 0.05$ compared with respective H_2O_2-treated cells.

boiled and resolved on 4–12% NuPage Bis-Tris acrylamide gels (Invitrogen/Life Technologies) and then transferred to nitrocellulose. Membranes were blocked in 10% nonfat dried milk and probed overnight with anti-RNF146 (Abnova, Walnut, CA, USA), PARP-1 (Cell Signaling Technology, Danvers, MA, USA), PAR (catalog number 528815, lot number D00057484; Calbiochem, San Diego, CA, USA), ubiquitin (Cell Signaling Technology) or heat shock protein 70 (HSP70, Enzo Life Sciences, Farmingdale, NY, USA) antibodies (1:1,000). After incubation with peroxidase-conjugated secondary antibodies, the blots were detected on a charge-coupled device (CCD) camera–based detection system (GBox; Syngene USA, Frederick, MD, USA) with enhanced chemiluminescent substrate. To normalize signals, membranes were stripped in 62.5 mmol/L Tris, 2% SDS, 100 mmol/L β-mercaptoethanol at 60°C for 20 min, blocked and reprobed with antibodies against actin (Santa Cruz Biotechnology, Santa Cruz, CA, USA). The signals were quantitated by using the Genetools analysis software (Syngene USA).

Coimmunoprecipitation

PARP-1 was activated in confluent H9c2 cells grown in 6-cm culture dishes

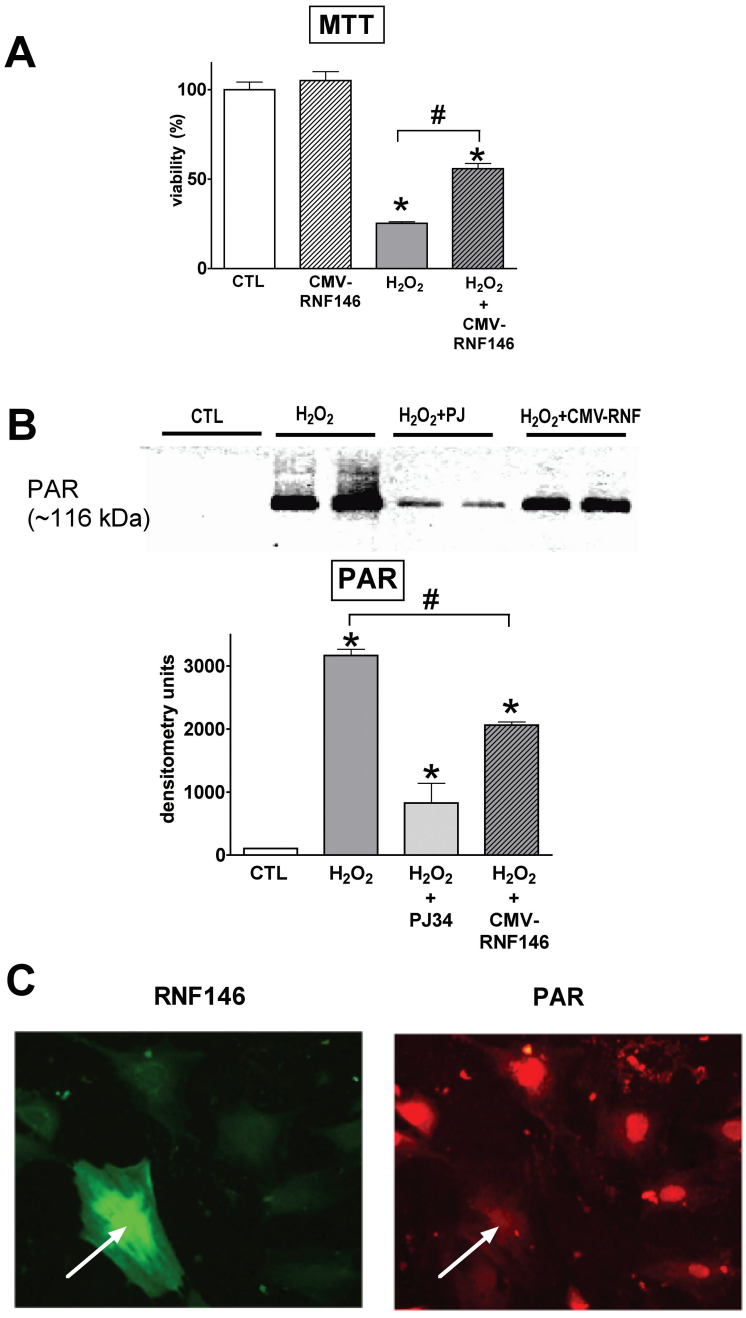

Figure 4. RNF146 overexpression is cytoprotective in transiently transfected cells. (A, B) 293T cells were transiently transfected with CMV-RNF146 vector (CMV-RNF) or empty pcDNA3.1$^+$ vector (CTL) and exposed to H_2O_2 to induce PARP-1 activation and cell death. (A) Cell viability was measured after 3 h by the MTT assay. (B) PARP-1 activation is measured at its the peak (5 min in 293T cells) by immunoblotting for poly(ADP-ribose) (PAR) polymer at 116 kDa. The PARP inhibitor PJ34 (3 μmol/L) was used in pretreatment (30 min). Representative blot image and densitometric analysis results are shown. (C) H9c2 cells were transiently transfected with pcDNA-RNF146 and exposed to H_2O_2 (600 μmol/L, 30 min, peak of PARP activation in H9c2 cells). Cells were fixed and immunostained for RNF146 (left panel) and PAR polymer (right panel). Decreased PAR signal was detectable (right panel, arrow) in cells showing RNF146 overexpression (left panel, arrow).

by exposure to H_2O_2 in fresh culture medium. Control cells were pretreated with PARP inhibitor PJ34 (3 μmol/L, 30 min) and received fresh culture medium without H_2O_2. Cells were lysed and scraped in lysis buffer (100 mmol/L HEPES, 200 mmol/L NaCl, 40 mmol/L EDTA, 4 mmol/L EGTA, 100 mmol/L NaF, 20 mmol/L β-glycerophosphate, 2 mmol/L Na_3VO_4, 2% Triton X-100) supplemented with protease inhibitors (Complete Mini EDTA-free) on ice. Cell lysates were centrifuged at 16,000 × *g* for 10 min, and the cleared lysate was used for direct immunoprecipitation by using the Dynabeads Protein G Immunoprecipitation Kit (Life Technologies). Antibodies recognizing the N terminus of RNF146 (Abnova), residues surrounding Gly623 of PARP-1 (Cell Signaling Technology) or ubiquitin (Cell Signaling Technology) were incubated with Protein G Dynabeads for 1 h at 4°C to allow them to bind to magnetic beads. The antibody–Dynabeads complexes were incubated with 2× diluted cell lysates for 1 h at 4°C. The captured complexes were thoroughly washed and eluted under denaturing conditions. Samples were analyzed by Western blotting by using antibodies recognizing different parts of the proteins: the C terminus of RNF146 (Aviva Systems Biology, San Diego, CA, USA) and the region surrounding Gly215 of PARP-1 (Cell Signaling Technology) and protein-A-HRP conjugate (Amersham/GE Healthcare, Life-Sciences, Pittsburgh, PA, USA).

Immunocytofluorescence

H9c2 cells were plated (50,000/well) on Lab-Tek™ II eight-well chamber slides (Nalge Nunc, Rochester, NY, USA) and cultured until they reached confluency. They were exposed to H_2O_2 (1 mmol/L, 30 min) or vehicle and fixed in 4% neutral buffered formalin for 15 min. Cells were permeabilized with 0.2% Triton X-100, blocked with 2.5% horse serum (Vector Laboratories, Burlingame, CA, USA) and probed with PARP-1 (1:100; Cell Signaling Technology) or RNF-146 antibody (1:100, Abnova,

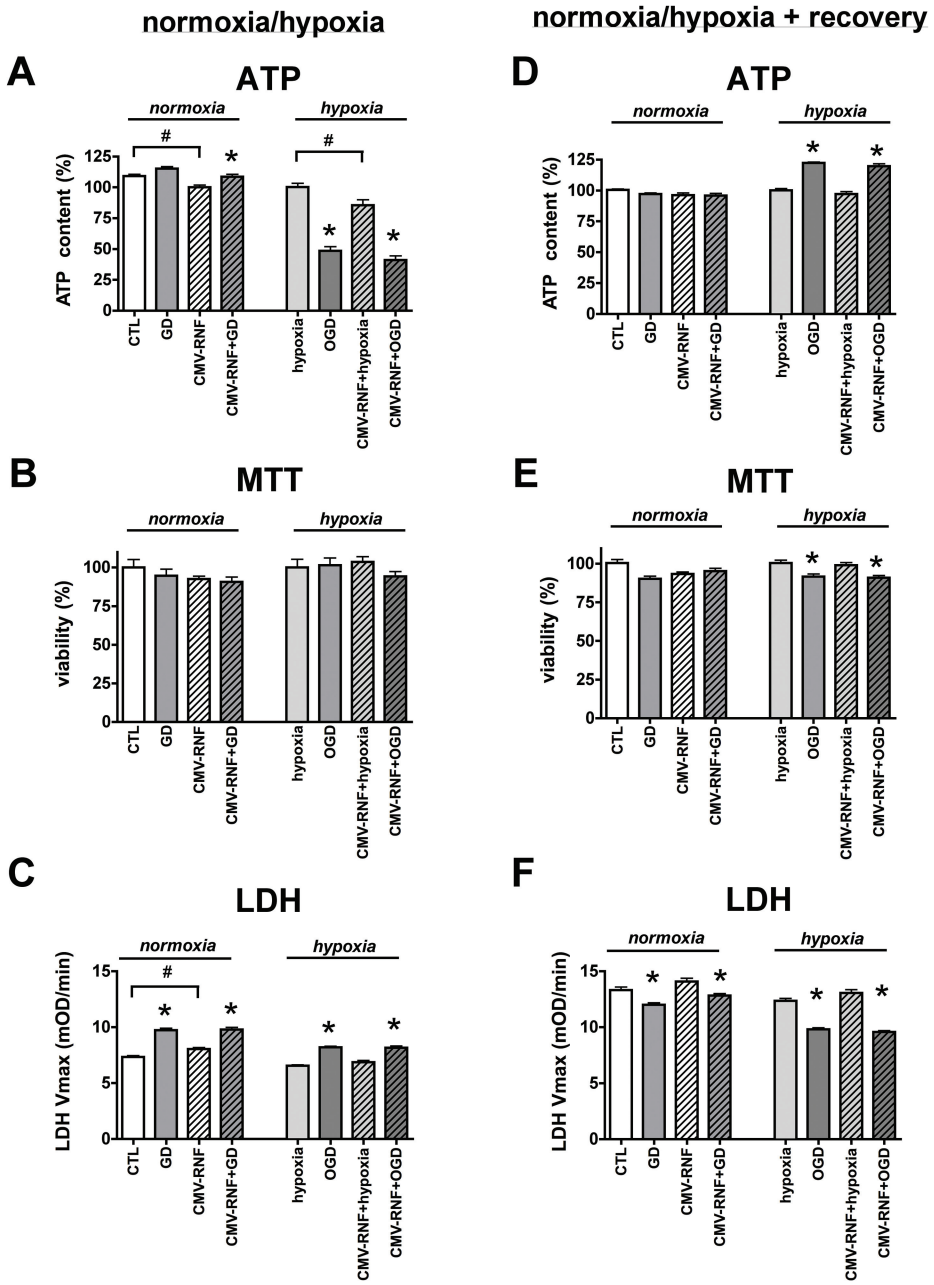

Figure 5. RNF146 overexpression provides no protection against ATP depletion induced by oxygen-glucose deprivation (OGD). (A–F) RNF146 was overexpressed in H9c2 cells (CMV-RNF) by stable transfection with pcDNA-RNF146. Control cells (CTL) were simultaneously transfected with β-galactosidase expression vector and selected with G418. Cells were subjected to hypoxia, glucose deprivation (GD) or oxygen-glucose deprivation (OGD) or maintained at normoxia with regular culture medium for 8 h (A–C) followed by 16 h of recovery (D–F) with normalization of glucose concentration and oxygen tension. Cellular ATP content (A, D), MTT-converting capacity (B, E) and lactate dehydrogenase (LDH) release (C, F) are shown. $^{*}p < 0.05$ compared with respective normoxic or hypoxic condition; $^{\#}p < 0.05$ CMV-RNF cells compared with CTLs.

Walnut, CA) followed by incubation with Alexa Fluor 546–labeled secondary antibody (Invitrogen/Life Technologies). The cells were subsequently stained with nuclear stain Hoechst 33342 and Alexa Fluor 488 phalloidin conjugate, and after extensive washing, coverslips were applied with Mowiol. (Alexa Fluor 488 secondary label was used to detect RNF146 when no phallodin staining was performed.) Images were taken on an Eclipse 80i fluorescent microscope (Nikon Instruments, Melville, NY, USA) with a Coolsnap HQ^2 14-bit CCD camera (Photometrics, Tucson, AZ, USA). PARP-1 staining intensity was evaluated by a NIS Elements software package (Nikon Instruments). The nuclear area was recognized on a Hoechst 33342 channel, and applying this binary layer to the PARP-1 channel fluorescence intensity was measured in the nuclear and extranuclear areas. The ratio of nuclear and extranuclear areas remained unchanged after H_2O_2 exposure on the images evaluated.

Ischemia-Reperfusion Injury

Balb/c male mice (n = 10) were anesthetized and myocardial ischemia was produced by occlusion of the left anterior descending (LAD) coronary artery as described (15). After 30 min of LAD coronary artery occlusion, the ligature was removed, and reperfusion was visually confirmed. The hearts were reperfused for 2 h and were processed for histology in half of the animals. The ischemic area (area at risk) was separated from the nonischemic parts and processed separately. Mouse heart samples were fixed in 4% neutral buffered formalin and embedded in paraffin. The 4-μm sections were cut and the slides were stained with hematoxylin and eosin, with Masson trichrome stain technique or subjected to immunohistochemistry for PARP-1, PAR and RNF146. In the remaining animals, reperfusion was allowed for 3 h and the heart samples were used for quantitative analysis by Western blotting. Sham-operated control mice (n = 10) were subjected to anesthesia and surgical

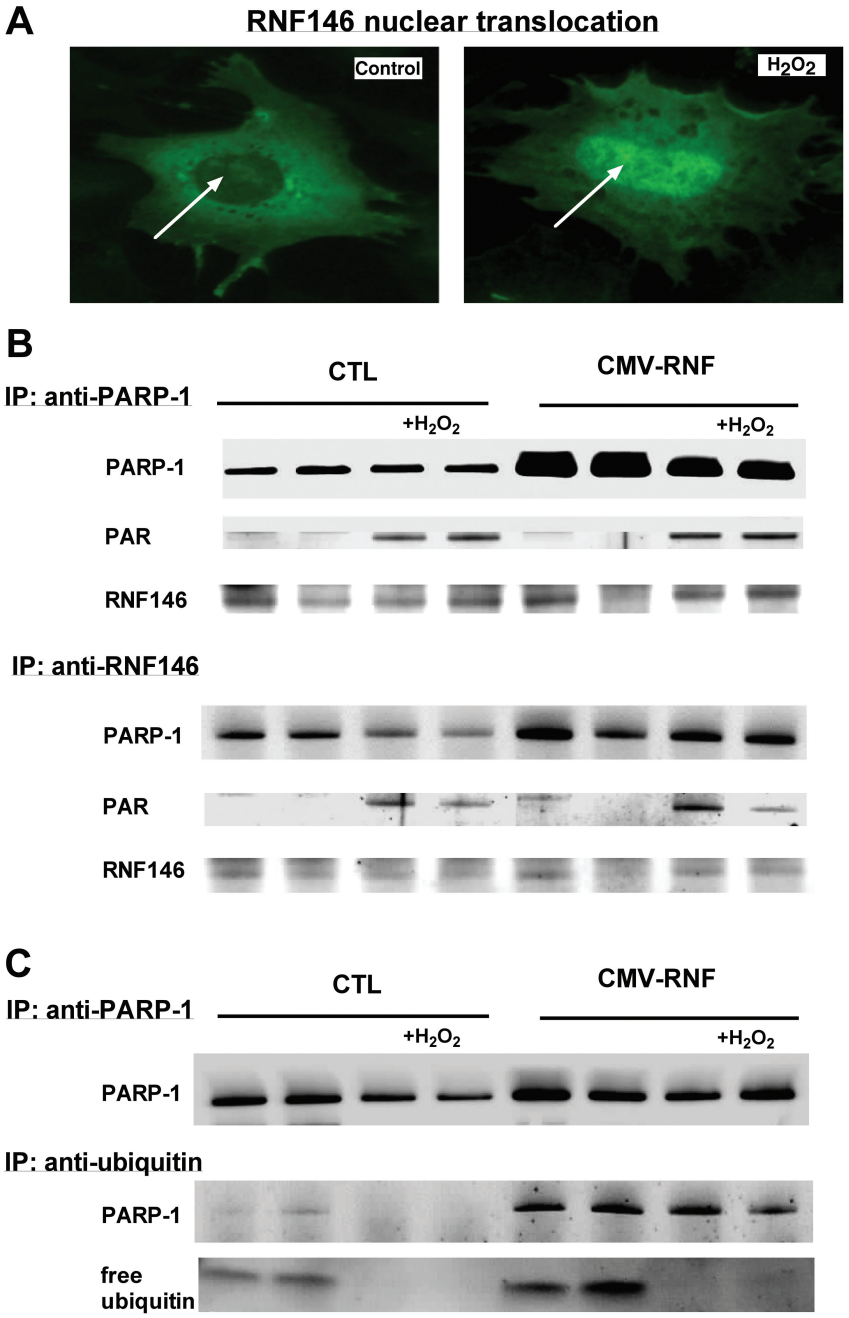

Figure 6. RNF146 directly interacts with PARP-1. (A) Nuclear translocation of RNF146 is detected in H9c2 cardiomyoblasts exposed to H_2O_2 (600 μmol/L, 30 min). The cells were fixed in formalin, stained with RNF146 antibody and visualized with Alexa Fluor 488–labeled secondary antibody. Resting cells show cytoplasmic staining, whereas intense nuclear staining is detectable in cells exposed to H_2O_2. (B, C) H9c2 cells stably transfected with RNF146 (CMV-RNF146) or with control vector (CTL) were exposed to H_2O_2 (1 mmol/L, 30 min). (B) Immunoprecipitation (IP) was performed with PARP-1 or RNF146 antibodies, and the presence of PARP-1 and RNF146 proteins and activation of PARP-1 (PARylation at 116 kDa, PAR) were tested by Western blotting. Interaction of RNF146 and PARP-1 (both PARylated and non-PARylated forms) was detected. (C) Immunoprecipitation by PARP-1 and ubiquitin antibodies was followed by Western blotting for PARP-1 and ubiquitin and revealed PARP-1 ubiquitination and the consumption of free ubiquitin.

procedures except for LAD coronary artery occlusion and samples were processed simultaneously.

Immunohistochemistry

Immunohistochemical staining was performed as previously described (16,17). Mouse heart samples were fixed in 4% neutral buffered formalin and embedded in paraffin. The 4-μm sections were cut and picked up on adhesive slides. Endogenous peroxidase activity was suppressed on deparaffinized and rehydrated sections by treating slides with H_2O_2 (0.6% in methanol, 15 min). Antigenic epitopes were retrieved by microwaving the sections in citrate buffer (0.2 mol/L citrate, pH 3.0, for PAR or 10 mmol/L citrate, pH 6.0, for all other antigens). Sections were blocked with normal horse serum (blocking serum) or with M.O.M. diluent (Vector Laboratories). Ig and protein blocking reagents (Vector Laboratories) in PBS contained 0.2% Triton X-100. Antibodies against PARP-1 (1:100; Bethyl Laboratories, Montgomery, TX, USA), PAR (1:200; Calbiochem) or RNF146 (1:100; Abnova) were applied in blocking serum or M.O.M. diluent, and sections were incubated overnight at 4°C. Sections were washed in PBS containing 0.2% Triton X-100 (wash buffer) and incubated with biotinylated anti-rabbit or anti-mouse antibodies (1:200), respectively. Then sections were washed and incubated with ABC peroxidase reagent (Vectastain Elite ABC kit; Vector Laboratories) for 30 min, and peroxidase sites were revealed with 3,3′-diaminobenzidine-tetrahydrochloride (DAB) and H_2O_2 (DAB substrate kit; Vector Laboratories). Slides were washed and counterstained with Hematoxylin QS (Vector Laboratories), dehydrated in an ascending alcohol series, cleared in xylene and coverslipped with Permount (Thermo Fisher Scientific Inc., Waltham, MA, USA). Negative control sections were simultaneously stained with the omission of primary antibodies.

Slides were viewed on an Eclipse 80i fluorescent microscope (Nikon Instruments) under bright-field illumination,

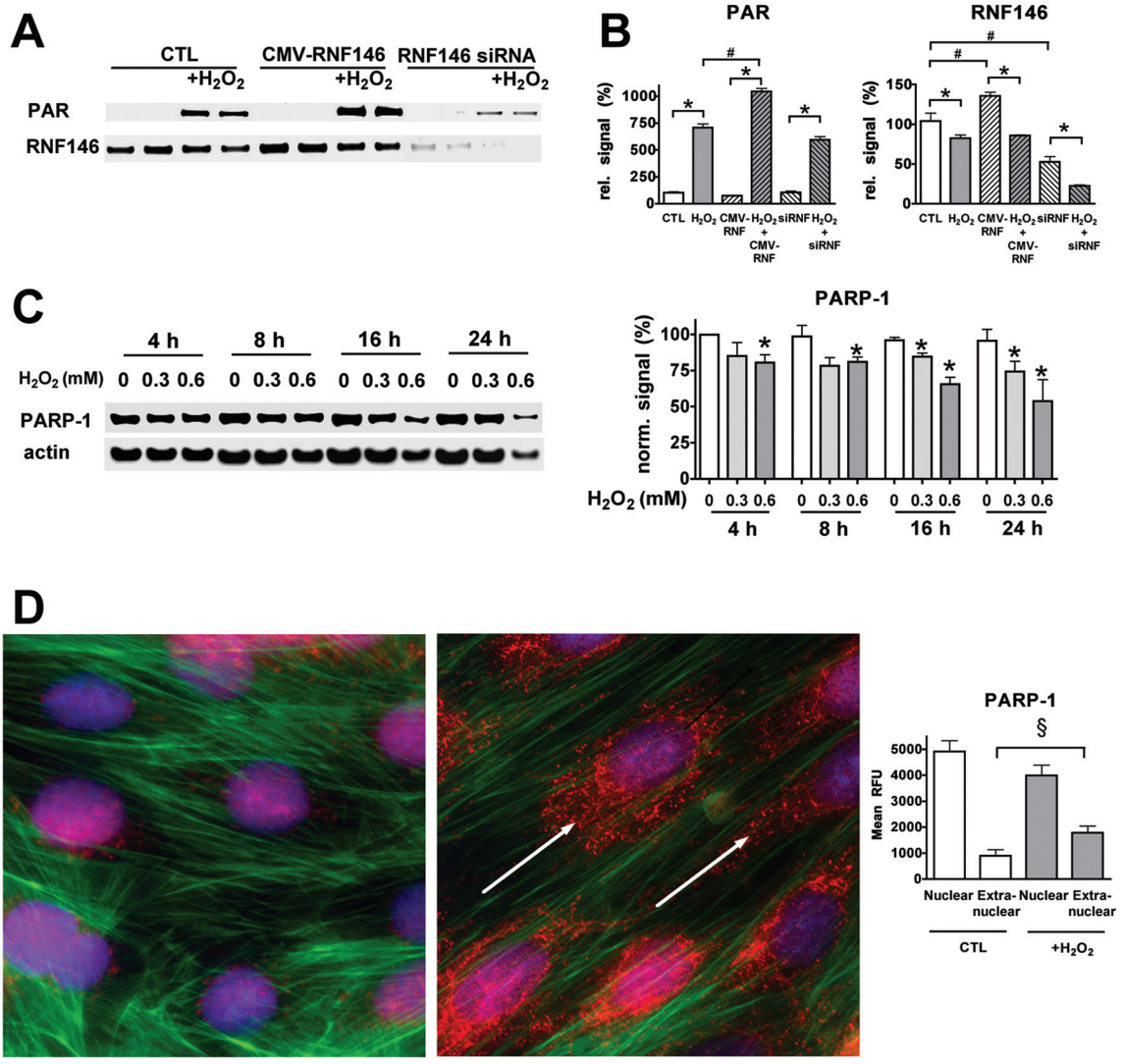

Figure 7. Oxidative stress decreases the levels of RNF146 and PARP-1 proteins and induces nuclear-to-cytoplasmatic PARP-1 release. (A, B) H9c2 cardiomyocytes stably transfected with CMV-RNF146 (CMV-RNF) or transfected with RNF146 siRNA (siRNF) and exposed to H_2O_2 (1 mmol/L, 30 min). PARP-1 activation (PARylation of PARP-1 at 116kDa, PAR) and the expression of RNF146 were measured by Western blotting. Representative blots (A) and results of densitometric analysis (B) are shown. (C) PARP-1 expression was measured in H9c2 cells after H_2O_2 injury (300 or 600 μmol/L) at 4, 8, 16 or 24 h. Immunoblots and densitometric analysis results are shown. $^{*}p < 0.05$ (H_2O_2 induced significant expression changes compared with respective controls) (B, C); $^{\#}p < 0.05$ compared with CTL cells (B). (D) PARP-1 is released from the nucleus and translocates to the cytoplasm in response to oxidative stress. H9c2 cells were exposed to H_2O_2 (1 mmol/L, 30 min) and fixed by neutral buffered formalin. PARP-1 immunostaining was visualized by using Alexa Fluor 546 (red). Actin filaments were stained with Alexa Fluor 488 phalloidin (green) and the nucleus with Hoechst 33342. The left panel shows control cells and the right panel shows cells exposed to H_2O_2. The mean fluorescence intensity (RFU) was measured in the nuclear and extranuclear regions to quantitate PARP-1 release from the nucleus. $^{\S}p < 0.05$ (H_2O_2 induced significant translocation of PARP-1 to the cytoplasm) (D).

and images were captured with a digital firewire camera system (DS-Vi1 Color digital camera; Nikon Instruments). Five images (area of 251 × 188 μm) were taken of all slides, and the positively stained and negative nuclei were counted. The percent positivity of nuclei is shown on the graphs.

Statistics

One-way analysis of variance (ANOVA) was used to detect differences between groups or unpaired two-tailed Student *t* test to compare two groups. *Post hoc* comparisons were made using the Tukey test. A value of $p < 0.05$ was considered statistically significant. The correlation analysis was performed by

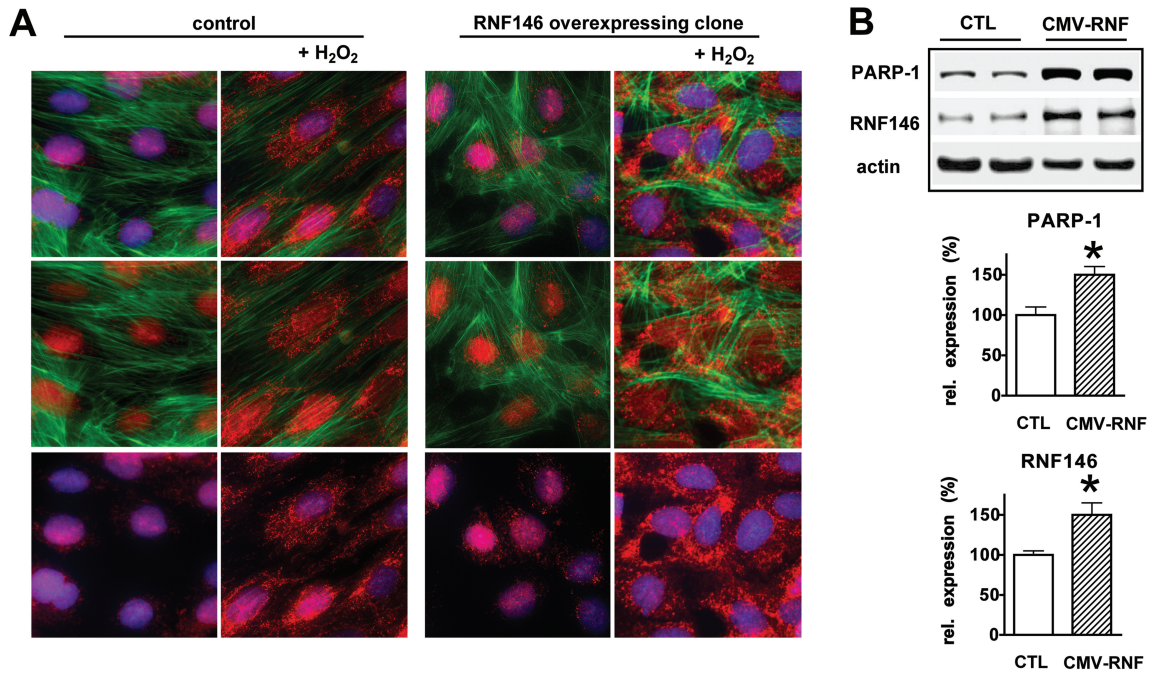

Figure 8. PARP-1 is released from the nucleus during oxidative stress: enhancement by RNF146 overexpression. (A, B) RNF146 was overexpressed in the cells by stable transfection with pcDNA-RNF146 (CMV-RNF146). Control cells (CTL) were simultaneously transfected with β-galactosidase expression vector and selected with G418. (A) H9c2 cells were exposed to H_2O_2 (1 mmol/L, 30 min) and fixed by neutral buffered formalin. PARP-1 immunostaining was visualized using Alexa Fluor 546 (red). Actin filaments were stained with Alexa Fluor 488 phalloidin (green) and the nucleus with Hoechst 33342 (blue). Left panel shows control cells and right panel shows cells exposed to H_2O_2. All three channels are merged on the top panels; the PARP-1 and phalloidin channels are merged in the middle ones and PARP-1 and Hoechst are merged on the bottom panels. (B) RNF146 and PARP-1 expression was measured by Western blotting in stably transfected cells and the signal was normalized to actin signal. Representative blot image and densitometric analysis results are shown; *$p < 0.05$ compared with the CTL.

linear regression analysis. All statistical calculations were performed by using Prism 4 analysis software (GraphPad Software, La Jolla, CA, USA). Data are shown as mean ± SEM (standard error of the mean) values.

RESULTS

RNF146 Protects Cardiomyocytes Against Oxidant-Induced Cell Death

RNF146 was expressed at high levels in various tissues, including the heart under basal conditions (Figure 1A), consistently with the previously reported high abundance of RNF146 mRNA in the heart (18). The protein was homogenously present in the cytoplasm of cardiomyocytes (Figures 1B–E) and exhibited a similar cytoplasmic localization in H9c2 cardiomyoblasts (Figures 1F, G).

Because RNF146 has previously been demonstrated to be protective against PARP-1–mediated cell death in neurons (see Introduction), we tested whether it exerts similar protection against oxidant injury in cardiomyocytes by using siRNA-mediated gene silencing and stable transfection of H9c2 cells with RNF146 expression vector (Figure 2). We found that H_2O_2-induced cell death was enhanced after RNF146 silencing (Figures 3A–C), while overexpression of the protein exerted cytoprotection against the oxidant-mediated injury in H9c2 cardiomyocytes (Figures 3D–F). Consistently with previous findings showing that the protection exerted by RNF146 depends on PARP-1 activation (9), RNF146 silencing no longer potentiated cell death in the presence of the competitive PARP inhibitor compound (19) PJ34 (Figures 3B, C). Furthermore, RNF146 overexpression did not exert additional protective effects in PJ34-treated cells (Figures 3E, F). Cell survival was also increased by RNF146 in transiently transfected 293T cells subjected to oxidant injury, but PARP-1 activation (detected as PARylation of PARP-1) was only mildly affected (Figures 4A, B). The PAR signal was decreased in H9c2 cells transiently transfected with RNF146 exposed to H_2O_2, and it coincided with a strong nuclear RNF146 signal (Figure 4C).

In H_2O_2 injury, necrotic cell death occurs in cardiomyocytes as a result of PARP-1 (over)activation that rapidly depletes the cellular NAD^+ and ATP pools (1–6,12,21,22). The cellular NAD^+ and ATP content can also be depleted without PARP-1 activation by oxygen-glucose deprivation (OGD), but in a manner that

is largely unrelated to PARP-1 overactivation (13,14,20). As expected, in this model, RNF146 overexpression did not affect the changes in cellular viability (Figure 5). Taken together, these data suggest that RNF146 acts downstream of PARP-1 activation (PAR polymer generation) in cardiomyocytes, and its role is more predominant during oxidant-mediated cell death than in hypoxic-ischemic conditions.

RNF146 Directly Interacts with PARP-1, and the Levels of Both Proteins Decrease in Oxidative Stress

As mentioned in the Introduction, RNF146 was initially recognized as a cytoplasmic PAR binding protein that can capture PAR polymers and protects neurons against the PAR polymer-induced cell death (parthanathos). In our cardiomyocyte model, however, RNF146 had a protective effect in the early (necrotic) phase of oxidant injury without blocking the activation of PARP-1. Because the intracellular NAD^+ pools are compartmentalized (9,23,24), the mechanisms by which PARP-1 can exhaust the cytoplasmic NAD^+ compartment remain incompletely understood. Still, a significant degree of cellular NAD^+ and ATP depletion occurs after PARP-1 activation in oxidant injury, and depletion of cytosolic NAD^+ is required for cell death, since restoration of cytosolic NAD^+ content is sufficient to prevent PARP-1–mediated cell death (25). We hypothesized that RNF146 may uncouple PARP-1 activation from the loss of NAD^+ in the cytoplasm by interfering with a PARylated "signaling molecule." Because PARP-1 is the most abundantly PARylated protein in oxidative stress, we tested whether RNF146 can interact with PARP-1. Under basal conditions, PARP-1 is primarily nuclear and, in some cells, mitochondrial (26–28), whereas RNF146 is cytoplasmic. No interaction is expected between the two proteins. We tested whether the localization of RNF146 may change in oxidative stress, since a nuclear translocation of the overexpressed RNF146 was observed by us in cardiomyocytes (Figure 4C) and by others in neurons (8). We found that endogenous RNF146 also translocates to the nucleus upon H_2O_2 stimulation (Figure 6A).

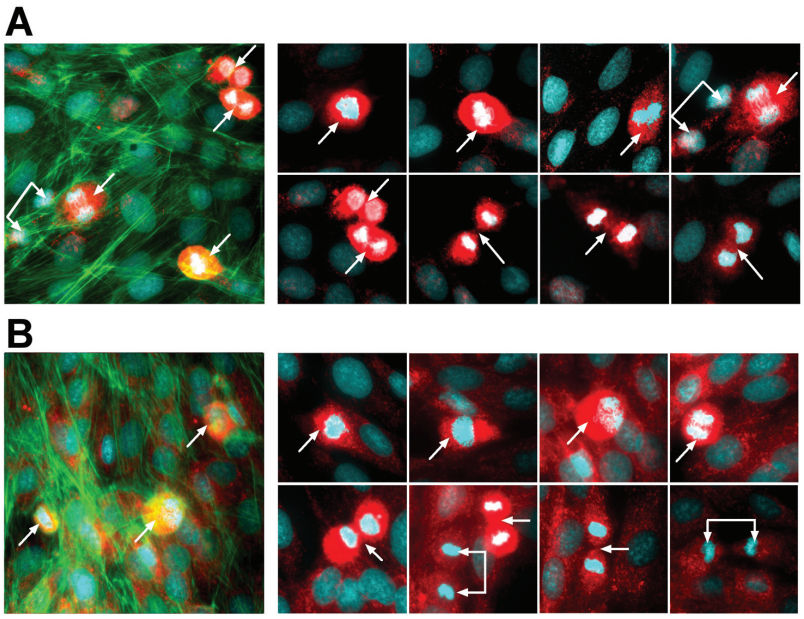

Figure 9. PARP-1 release from the nucleus coincides with increased RNF146 expression during mitosis. (A) H9c2 cells were immunostained with PARP-1 and Alexa Fluor 546 secondary antibodies (red); nuclei were labeled with Hoechst 33342 (blue) and actin with Alexa Fluor 488 phalloidin (green). Mitotic phases are shown with merged Hoechst and PARP-1 channels; dividing cells are labeled with arrows. Intense cytoplasmic PARP-1 staining is observed from prometaphase (when the nuclear membrane disintegrates) to anaphase. PARP-1 staining intensity decreases by the telophase (when new nuclear membrane is formed) in the two daughter cells (connected arrows). (B) H9c2 cells were immunostained with RNF146 and Alexa Fluor 546 secondary antibodies (red); nuclei were labeled with Hoechst 33342 (blue) and actin with Alexa Fluor 488 phalloidin (green). Mitotic phases are shown with merged Hoechst and RNF146 channels; dividing cells are labeled with arrows. RNF146 staining intensity is increased in dividing cells from prometaphase to anaphase. RNF146 staining intensity decreases in the two daughter cells (connected arrows) in the telophase.

To test the potential of a direct interaction between RNF146 and PARP-1, coimmunoprecipitation assays were performed. Immunoprecipitation by PARP-1 antibody pulled down RNF146, whereas immunoprecipitation with RNF146 antibody pulled down PARP-1 in both RNF146 overexpressing and normal control cells (Figure 6B). Interestingly, the interaction between the two proteins did not appear to be enhanced when the auto-PARylation of PARP-1 increased. RNF146 overexpression increased the amount of PARP-1 in the precipitate either using RNF146 or PARP-1 antibody for pull-down.

RNF146 was reported to act as an E3 ubiquitin ligase, which is the protein that confers substrate specificity in the ubiquitin-proteasome system: it targets specific protein substrates for degradation (10,29,30). To test whether PARP-1 is ubiquitinated, we also performed the precipitation with anti-ubiquitin antibody that also pulled down PARP-1 from the RNF146 overexpressing cells and to a smaller extent from control cells (Figure 6C). The amount of detectable PARP-1 was lower in the samples exposed to H_2O_2 (1 mmol/L, 30 min), and free ubiquitin completely disappeared from them.

Next, we measured whether the amount of RNF146 decreases on H_2O_2-induced PARP-1 activation in normal control cells, in RNF146-silenced and in

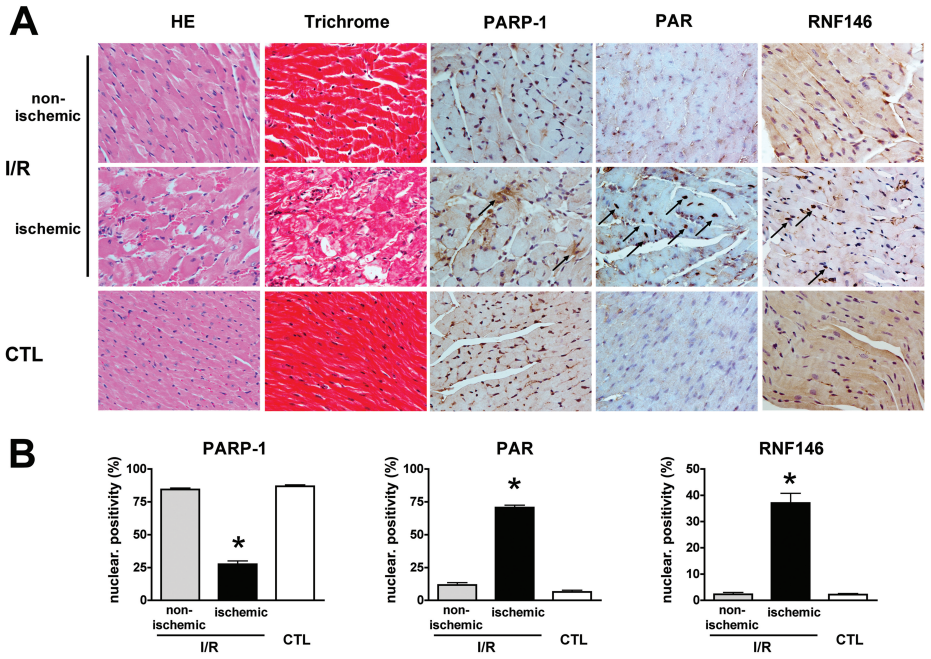

Figure 10. Ischemia-reperfusion injury induces the cytoplasmic release of PARP-1 and the nuclear translocation of RNF146 *in vivo*. (A, B) Regional ischemia-reperfusion injury was induced in mouse hearts by occlusion of the LAD coronary artery for 30 min; then the ligature was removed and the hearts were reperfused for 2 h. The ischemic and nonischemic areas of hearts subjected to ischemia-reperfusion (I/R) injury and sham-operated (CTL) hearts were fixed in formalin and embedded in paraffin. Sections were stained with hematoxylin and eosin (HE), Masson trichrome stain and immunostained with PARP-1, PAR or RNF146 antibodies. (A) Mild structural changes are detectable on HE- and trichrome-stained sections. PARP-1 immunostaining shows decreased nuclear staining with areas of extranuclear positivity (arrows). PARP-1 activation was detectable as nuclear positivity with PAR antibody (arrows). Nuclear translocation of RNF146 (marked with arrows) and diminished cytoplasmic staining was detectable. (B) Nuclear positivity was evaluated on five areas of each immunostained section and expressed as percentage values of PARP-1, PAR and RNF146 positivity (n = 5/group, $*p < 0.05$ compared with CTL).

RNF146-overexpressing cells. We found that RNF146 level rapidly decreases on oxidant exposure (1 mmol/L H_2O_2, 30 min) irrespective of its basal level (Figures 7A, B). RNF146 did not block PARP-1 activation, but the detectable PAR signal was slightly affected by RNF146 expression: it was highest in RNF146 overexpressing cells and lowest in RNF146 silenced cells.

Next, we tested whether PARP-1 level also decreases on less severe oxidant exposure and found that a noncytotoxic, lower concentration of H_2O_2 (0.3 mmol/L) significantly decreases its expression level over longer periods, although it has a lesser effect than a concentration that also causes cell death (Figure 7C). Because the data obtained so far showed that (a) RNF146 translocates to the nucleus upon oxidative stress, (b) directly interacts with PARP-1 and (c) the level of both proteins rapidly decreases in oxidatively stressed cells, we next tested whether PARP-1 exits to the cytoplasm during H_2O_2 induced myocyte injury. We found that the amount of nuclear PARP-1 decreases after exposure to H_2O_2, but it becomes detectable in the cytoplasm (Figure 7D). The release of PARP-1 from the nucleus was enhanced in RNF146 overexpressing cells (Figure 8). Interestingly, we have also noted that the nuclear membrane disintegrates during normal mitosis (that is, in the absence of oxidative stress), PARP-1 is also released from the nucleus into the cytoplasm; this coincides with increased RNF146 expression followed by rapid decrease of both proteins (Figure 9).

RNF146 Undergoes Nuclear Translocation in Myocardial Ischemia-Reperfusion Injury *In Vivo* and PARP-1 Is Consumed

As discussed in the Introduction, PARP-1 activation occurs in the reperfused myocardium in ischemia-reperfusion injury and PARP inhibitors exert cardioprotective effects. Interestingly, all prior histochemical studies focused on the localization of PAR (the product of the enzyme); surprisingly, neither the expression level nor the localization of PARP-1 itself has been previously studied during myocardial ischemia-reperfusion injury. Therefore, we examined the localization of PARP-1 and RNF146 in mice subjected to myocardial ischemia-reperfusion injury. After 30 min of ischemia (occlusion of the left descending coronary artery), followed by 2 h of reperfusion, the amount of nuclear PARP-1 decreased, and regions of intense cytoplasmic PARP-1 staining appeared in the ischemic area (area at risk) (Figures 10A, B). Strong PARP-1 activation was still detectable in the nucleus by immunostaining for PAR (the reaction product of PARP-1 activity), even though the nuclear levels of the PARP-1 enzyme markedly decreased. Concomitant with these changes, a significant amount of cytoplasmatic-to-nuclear translocation of RNF146 was observed in the ischemic region. No change was detected in either PARP-1 or RNF146 expression or localization in the nonischemic regions of the heart subjected to regional ischemia.

Western blotting analysis performed in homogenates of the ischemic/reperfused heart and the corresponding nonischemic tissue revealed that the total amount of PARP-1 and RNF146 decreased in the ischemic regions of the heart after ischemia-reperfusion injury, and a similar decrease

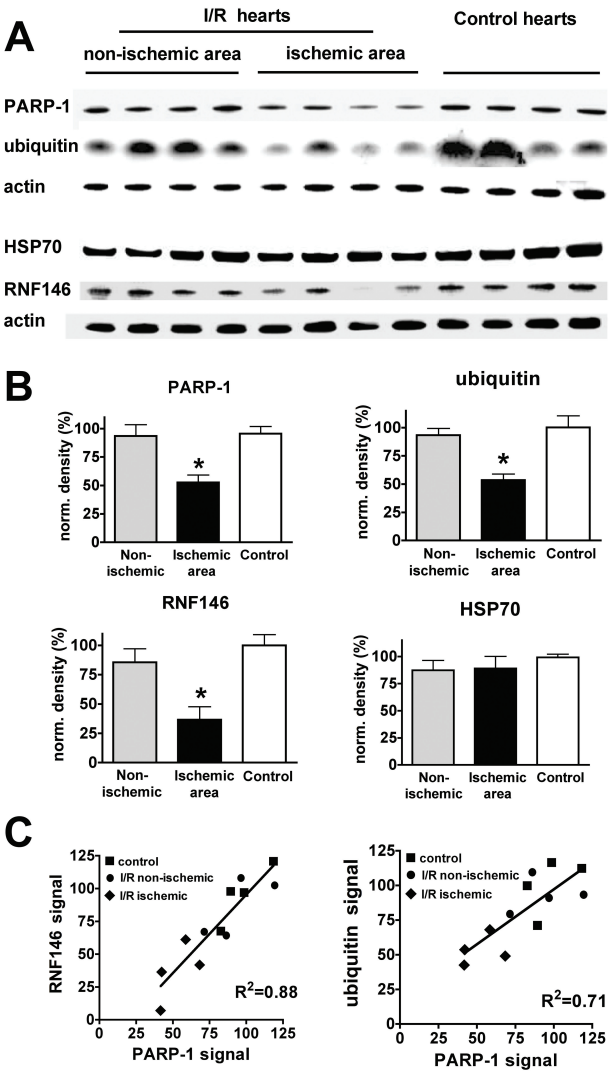

Figure 11. Ischemia-reperfusion injury results in an overall decrease in RNF146 and PARP-1 content in the myocardial tissue *in vivo*. (A–C) Ischemia-reperfusion (I/R) injury was induced in mouse hearts by LAD coronary artery occlusion for 30 min, followed by a 3-h reperfusion. Levels of PARP-1, RNF146, free ubiquitin and HSP70 were measured by Western blotting in the ischemic and nonischemic areas of I/R hearts and sham-operated (CTL) hearts. (A) Representative blot images and respective actin normalization signals are shown. (B) Densitometric analysis results of normalized values of PARP-1, RNF-146, free ubiquitin and HSP-70 are shown. n = 4/group. *$p < 0.05$ compared with CTL. (C) Correlation analysis was performed between the normalized levels of RNF146 and PARP-1 (left panel) or ubiquitin and PARP-1 (right panel). Linear regression curves and correlation coefficient (R^2) values are shown. (Values of control hearts are labeled with squares, the ischemic areas with diamonds and the nonischemic areas with filled circles.)

was observed in the amount of free ubiquitin (Figures 11A, B). The amount of heat shock protein 70 (HSP70) remained unchanged, indicating that degradation of PARP-1 and RNF146 is an early event after PARP-1 activation. PARP-1 and RNF146 levels showed a strong correlation, and a similar correlation was noted between the amount of PARP-1 and that of free ubiquitin (Figure 11C). These data, coupled with the conclusions based on the results of our *in vitro* studies in oxidatively stressed cardiac myocytes, and based on published data implicating the active role of RNF146 in ubiquitin-mediated protein degradation (29,30), suggest that (a) rapid consumption of PARP-1 and RNF146 occurs in the postischemic myocardium and (b) PARP-1 is destined for degradation after its activation, and RNF146 is the specific interacting protein that promotes its proteasomal inactivation (Figure 12).

DISCUSSION

The main findings and conclusions of the present study are the following: (a) RNF146, a cytoplasmic E3-ubiquitin ligase, acts as a direct interactor of PARP-1 in cardiac myocytes *in vitro*. (b) RNF146 modulates oxidative cell death; its overexpression protects against cell injury, whereas cell injury is augmented after RNF146 silencing in cardiac myocytes *in vitro*. (c) RNF146 translocates to the nucleus concomitantly with oxidant-induced PARP-1 activation, resulting in the nuclear-to-cytoplasmatic translocation of PARP-1, followed by the degradation of both proteins in cardiac myocytes *in vitro*. (d) The same processes also occur *in vivo*, where PARP-1 and RNF146 degradation occurs in the early phase of myocardial ischemia-reperfusion injury.

The original working model that stipulated that oxidant-mediated DNA injury promotes necrotic type cell death via PARP-1 overactivation and associated metabolic catastrophe due to NAD^+ and ATP depletion and mitochondrial dysfunction (31–35) has been further advanced and refined over the last two decades in several different ways. First, the above-mentioned mechanisms have been investigated in the context of caspase-mediated PARP-1 degradation, a well-known phenomenon that occurs in oxidatively stressed and dying cells. It has been demonstrated that caspase activation, and the consequent proteolytic PARP-1 degradation, in fact, serves to protect cells from an overwhelming degree of cell necrosis, and the intracellular energetic pools that are saved in the cell

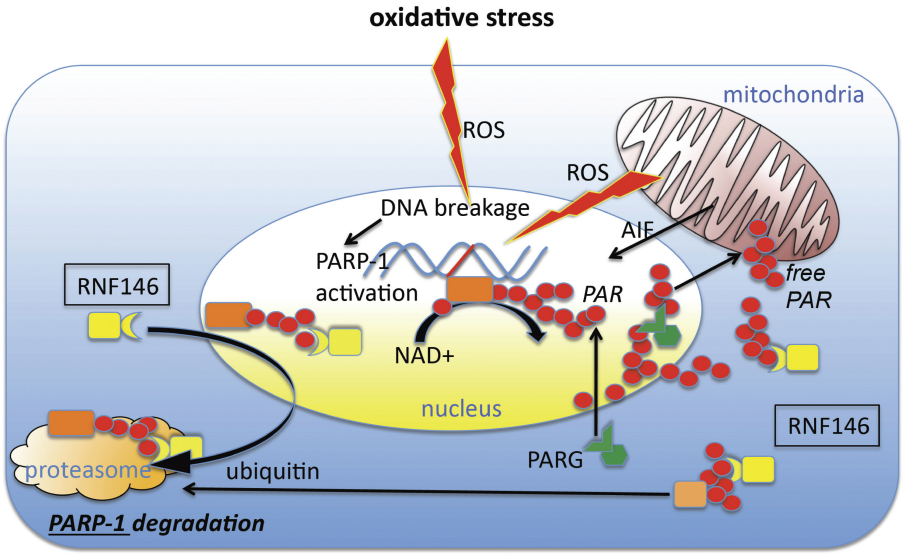

Figure 12. RNF146 controls PARP-1 degradation in oxidative stress. PARP-1 activation is triggered by DNA strand breaks in oxidative stress. The enzyme possesses high catalytic activity, builds large poly(ADP-ribose) (PAR) polymers on target proteins and can deplete the cellular NAD^+ pool, which contributes to necrotic cell death. Alternatively, PARP-1 activation can induce cell death in a delayed fashion by disrupting the nuclear and/or mitochondrial membranes by the negative charge of PAR polymers or by triggering the opening of the mitochondrial permeability transition pore that leads to the nuclear translocation of AIF (10). The major enzyme responsible for PAR catabolism is the cytoplasmic poly(ADP-ribose) glycohydrolase (PARG), which needs to translocate to the nucleus to access the PAR polymers. RNF146 is a protein that is normally cytoplasmatic (where it can capture PARylated proteins; based on the current results, during ischemia, PARP-1 can be translocated into the cytoplasm, and it can act as one of its interacting proteins). Moreover, the current results show that it can also rapidly translocate into the nucleus to directly interact with PARP-1. As an E3-ubiquitin ligase, RNF146 promotes the rapid proteasomal degradation of PARP-1. Thus, it irreversibly inactivates PARP-1. We hypothesize that this process may serve as a protective mechanism to limit the cellular/mitochondrial dysfunction induced by PARP-1 overactivation.

after PARP-1 cleavage are then used to execute apoptosis (36–38). Apoptosis, in this context, can be viewed as a mode of cell death that is more favorable than necrosis, because the various intracellular cell constituents, many of which serve as damage-associated molecules, are not released into the extracellular environment. A further refinement in the concept of PARP-1–mediated cell death was related to the discovery that a mitochondrial isoform of PARP-1 also exists (at least in some cell types) and may play an active role in oxidative cell injury (26–28). Another important finding was the recognition that PAR (the product of PARP) can be released into the cytoplasm from the nucleus and can directly act on the mitochondria to induce the release of apoptosis-inducing factor (AIF), which in turn induces nuclear DNA damage (39–42). Whereas this mechanism was originally recognized in neurons, subsequently, it was demonstrated in oxidatively stressed cardiac myocytes (43,44). The PARP-1 activation/PAR/AIF-mediated cell death, which has elements of both necrosis and apoptosis, is now also considered a distinct mode of cell death (parthanathos) (8,39). A systematic search for downstream regulators of parthanathos identified RNF146 (also termed "Iduna") (9). In an independent line of studies, RNF146 (in this study, it was also called "dactylidin") was simultaneously identified as a differentially expressed protein in the vulnerable regions of the brain in Alzheimer's disease; in this study, its E3 ubiquitin ligase function was also suggested (18).

The initial functional role of RNF146 was first demonstrated in neuronal models of cell death induced by NMDA receptor agonists. RNF146 was found to be neuroprotective against glutamate NMDA receptor–mediated excitotoxicity both *in vitro* and *in vivo* and against stroke (9). The major mechanism responsible for the protective effects was attributed to its ability to directly interfere with the PAR polymer (and its downstream effects such as AIF release and cell death), because the protective effects of RNF146 were attenuated by mutation at its PAR polymer-binding site (9). However, subsequent work revealed a more complex role of RNF146 in its interactions with PARP-1. For example, Zhang *et al.* (30) demonstrated that the interaction of RNF146 with PAR promotes the degradation of PARylated proteins. This effect was attributed to the interaction of PAR with the WWF domain of RNF146; the enhanced degradation of PARylated proteins (as shown with several PARylated proteins, such as axin, tankyrase and PARP-1) was found to occur through ubiquitination and subsequent degradation through the proteasome (10,46). Another line of work demonstrated that the E3 ligase function of RNF146 is increased by PAR binding, and this PAR binding leads to the ubiquitination of the associated proteins (as demonstrated with PARP-1, X-ray repair cross-complementing protein 1 [XRCC1], DNA ligase III and Lupus Ku autoantigen protein p70 [Ku70]). The PAR-dependent, RNF146-mediated ubiquitination of PARP-1 has been demonstrated to target PARP-1 for proteasomal degradation (47,48). It is noteworthy that the ubiquitination of PARP-1 has already been noted in prior studies as well (49), although without exploring the potential role of RNF146 in this process.

Curiously, the subcellular compartmentalization of PARP-1 was not addressed in these prior studies, even though it was generally assumed that PARP-1 is primarily nuclear, and RNF146 is exclusively cytoplasmatic. The previous state-of-the-art of parthanathos specified that PAR (that is, the product of PARP-1), but not PARP-1 enzyme itself, undergoes nuclear-to-cytoplasmatic translocation. The results of the current study (admittedly, in a different cell type and cell injury model, which makes direct comparisons difficult) confirm and extend some of these previous observations and may even resolve some of the above-mentioned dilemmas. First, the studies in the current report confirm the direct interaction of PARP-1 and RNF146. (Although in our experiments the intensity of the pull-down did not increase when the auto-PARylation of PARP-1 increased, this does not necessarily exclude the possibility that this interaction occurs through PAR, since PARP-1 has some degree of basal auto-PARylation. However, other mechanisms [for example, a direct protein-protein interaction] may also be possible). Second, the results of the current study confirm the RNF146-mediated ubiquitination of PARP-1 and are consistent with the model whereby the RNF146-induced ubiquitination directs PARP-1 into the proteasome, thereby facilitating its degradation. Third, on the basis of novel results of the current study, we conclude that the interaction of RNF146 and PARP-1, at least in oxidatively stressed cardiomyocytes, involves the cytoplasmatic-to-nuclear translocation of RNF146, as well as the nuclear-to-cytoplasmatic exit of PARP-1. The present report provides evidence for these phenomena both in an *in vitro* oxidatively stressed cardiomyocyte model and in an *in vivo* myocardial ischemia-reperfusion model. We hypothesize that this mechanism (somewhat similarly to the caspase-mediated cleavage of PARP-1 mentioned earlier [36–38] and by the recently recognized degradation of PARP-1 by ADP-ribosyl-acceptor hydrolase 3 [50]) serves as a protective function during oxidant-mediated cell death, since it limits the degree of PARP-1 overactivation and the associated cellular energetic catastrophe and cell necrosis. Also, this mechanism may partially restore cellular energetic pools, perhaps in an attempt of the cell to switch the mode of cell death to a more regulated form (for example, apoptosis).

Activation of the ubiquitin-proteasome system was observed in ischemia-reperfusion injury, and proteasome inhibitors have been proposed to exert a cardioprotective role in myocardial infarction (51). However, in agreement with our results, no beneficial effect of proteasome inhibition was observed in short-term reperfusion injury (52). Thus, we hypothesize that the positive effects of proteasome inhibition may be related to the inhibition of inflammatory pathways.

CONCLUSION

On the basis of several lines of data in neurons (9,53) and on the basis of the current data in cardiac myocytes, we conclude that the amount of RNF146 in a cell directly and remarkably affects the fate of the cell during oxidative injury; high levels of RNF146 are protective, whereas low levels of RNF146 (for example, after siRNA-mediated silencing) exacerbate cell injury. Whereas many mechanistic details remain to be further defined, we propose that pharmacological upregulation/therapeutic induction of RNF146 may represent a future approach for experimental therapeutic intervention of oxidant-mediated cardiac injury.

ACKNOWLEDGMENTS

This work was supported by the National Institutes of Health (to C Szabo) (R01GM056687).

DISCLOSURE

The authors declare that they have no competing interests as defined by *Molecular Medicine*, or other interests that might be perceived to influence the results and discussion reported in this paper.

REFERENCES

1. Jagtap P, Szabo C. (2010) Poly(ADP-ribose) polymerase and the therapeutic effects of its inhibitors. *Nat. Rev. Drug Discov.* 4:421–40.
2. Curtin NJ, Szabo C. (2013) Therapeutic applications of PARP inhibitors: anticancer therapy and beyond. *Mol. Aspects Med.* 34:1217–56.
3. Zingarelli B, Cuzzocrea S, Zsengellér Z, Salzman AL, Szabo C. (1997) Protection against myocardial ischemia and reperfusion injury by 3-aminobenzamide, an inhibitor of poly (ADP-ribose) synthetase. *Cardiovasc. Res.* 36:205–15.
4. Zingarelli B, Salzman AL, Szabo C. (1998) Genetic disruption of poly (ADP-ribose) synthetase inhibits the expression of P-selectin and intercellular adhesion molecule-1 in myocardial ischemia/reperfusion injury. *Circ. Res.* 83:85–94.
5. Yang Z, Zingarelli B, Szabo C. (2000) Effect of genetic disruption of poly (ADP-ribose) synthetase on delayed production of inflammatory mediators and delayed necrosis during myocardial ischemia-reperfusion injury. *Shock.* 13:60–6.
6. Pacher P, Szabo C. (2008) Role of the peroxynitrite-poly(ADP-ribose) polymerase pathway in human disease. *Am. J. Pathol.* 173:2–13.
7. Krietsch J, *et al.* (2013) Reprogramming cellular events by poly(ADP-ribose)-binding proteins. *Mol. Aspects Med.* 34:1066–87.
8. Fatokun AA, Dawson VL, Dawson TM. (2014) Parthanatos: mitochondrial-linked mechanisms and therapeutic opportunities. *Br. J. Pharmacol.* 171:2000–16.
9. Andrabi SA, *et al.* (2011) Iduna protects the brain from glutamate excitotoxicity and stroke by interfering with poly(ADP-ribose) polymer-induced cell death. *Nat. Med.* 17:692–9.
10. Kang HC, *et al.* (2011) Iduna is a poly(ADP-ribose) (PAR)-dependent E3 ubiquitin ligase that regulates DNA damage. *Proc. Natl. Acad. Sci. U. S. A.* 108:14103–8.
11. Gero D, *et al.* (2013) Cell-based screening identifies paroxetine as an inhibitor of diabetic endothelial dysfunction. *Diabetes.* 62:953–64.
12. Gero D, *et al.* (2007) Oxidant-induced cardiomyocyte injury: identification of the cytoprotective effect of a dopamine 1 receptor agonist using a cell-based high-throughput assay. *Int. J. Mol. Med.* 20:749–61.
13. Szoleczky P, *et al.* (2012) Identification of agents that reduce renal hypoxia-reoxygenation injury using cell-based screening: purine nucleosides are alternative energy sources in LLC-PK1 cells during hypoxia. *Arch. Biochem. Biophys.* 517:53–70.
14. Szabo G, *et al.* (2011) Cardioprotective effects of hydrogen sulfide. *Nitric Oxide.* 25:201–10.
15. Yang Z, Zingarelli B, Szabo C. (2000) Crucial role of endogenous interleukin-10 production in myocardial ischemia/reperfusion injury. *Circulation.* 101:1019–26.
16. Radovits T, *et al.* (2007) Poly(ADP-ribose) polymerase inhibition improves endothelial dysfunction induced by reactive oxidant hydrogen peroxide in vitro. *Eur. J. Pharmacol.* 564:158–66.

17. Radovits T, *et al.* (2007) Single dose treatment with PARP-inhibitor INO-1001 improves aging-associated cardiac and vascular dysfunction. *Exp. Gerontol.* 42:676–85.
18. von Rotz RC, Kins S, Hipfel R, von der Kammer H, Nitsch RM. (2005) The novel cytosolic RING finger protein dactylidin is up-regulated in brains of patients with Alzheimer's disease. *Eur. J. Neurosci.* 21:1289–98.
19. Jagtap P, *et al.* (2002) Novel phenanthridinone inhibitors of poly (adenosine 5′-diphosphate-ribose) synthetase: potent cytoprotective and antishock agents. *Crit. Care Med.* 30:1071–82.
20. Modis K, Gero D, Nagy N, Szoleczky P, Toth ZD, Szabo C. (2009) Cytoprotective effects of adenosine and inosine in an in vitro model of acute tubular necrosis. *Br. J. Pharmacol.* 158:1565–78.
21. Modis K, *et al.* (2012) Cellular bioenergetics is regulated by PARP1 under resting conditions and during oxidative stress. *Biochem. Pharmacol.* 83:633–43.
22. Gero D, Szabo C. (2008) Poly(ADP-ribose) polymerase: a new therapeutic target? *Curr. Opin. Anaesthesiol.* 21:111–21.
23. Nikiforov A, Dolle C, Niere M, Ziegler M. (2012) Pathways and subcellular compartmentation of NAD biosynthesis in human cells: from entry of extracellular precursors to mitochondrial NAD generation. *J. Biol. Chem.* 286:21767–78.
24. Berger F, Lau C, Dahlmann M, Ziegler M. (2005) Subcellular compartmentation and differential catalytic properties of the three human nicotinamide mononucleotide adenylyltransferase isoforms. *J. Biol. Chem.* 280:36334–41.
25. Alano CC, *et al.* (2010) NAD^+ depletion is necessary and sufficient for poly(ADP-ribose) polymerase-1-mediated neuronal death. *J. Neurosci.* 30:2967–78.
26. Du L, *et al.* (2003) Intra-mitochondrial poly(ADP-ribosylation) contributes to NAD+ depletion and cell death induced by oxidative stress. *J. Biol. Chem.* 278:18426–33.
27. Lai Y, *et al.* (2008) Identification of poly-ADP-ribosylated mitochondrial proteins after traumatic brain injury. *J. Neurochem.* 104:1700–11.
28. Rossi MN, *et al.* (2009) Mitochondrial localization of PARP-1 requires interaction with mitofilin and is involved in the maintenance of mitochondrial DNA integrity. *J. Biol. Chem.* 284:31616–24.
29. Zhou ZD, Chan CH, Xiao ZC, Tan EK. (2011) Ring finger protein 146/Iduna is a poly(ADP-ribose) polymer binding and PARsylation dependent E3 ubiquitin ligase. *Cell Adh. Migr.* 5:463–71.
30. Zhang Y, *et al.* (2011) RNF146 is a poly(ADP-ribose)-directed E3 ligase that regulates axin degradation and Wnt signalling. *Nat. Cell Biol.* 13:623–9.
31. Szabo C, Zingarelli B, O'Connor M, Salzman AL. (1996) DNA strand breakage, activation of poly (ADP-ribose) synthetase, and cellular energy depletion are involved in the cytotoxicity of macrophages and smooth muscle cells exposed to peroxynitrite. *Proc. Natl. Acad. Sci. U. S. A.* 93:1753–8.
32. Virág L, Salzman AL, Szabo C. (1998) Poly(ADP-ribose) synthetase activation mediates mitochondrial injury during oxidant-induced cell death. *J. Immunol.* 161:3753–9.
33. Ha HC, Snyder SH. (1999) Poly(ADP-ribose) polymerase is a mediator of necrotic cell death by ATP depletion. *Proc. Natl. Acad. Sci. U. S. A.* 96:13978–82.
34. Szabo C. (2005) Mechanisms of cell necrosis. *Crit. Care Med.* 33 (12 Suppl.):S530–4.
35. Virág L, Robaszkiewicz A, Rodriguez-Vargas JM, Oliver FJ. (2013) Poly(ADP-ribose) signaling in cell death. *Mol. Aspects Med.* 34:1153–67.
36. Virág L, *et al.* (1998) Peroxynitrite-induced thymocyte apoptosis: the role of caspases and poly (ADP-ribose) synthetase (PARS) activation. *Immunology.* 94:345–55.
37. Herceg Z, Wang ZQ. (1999) Failure of poly(ADP-ribose) polymerase cleavage by caspases leads to induction of necrosis and enhanced apoptosis. *Mol. Cell. Biol.* 19:5124–33.
38. Soldani C, Scovassi AI. (2002) Poly(ADP-ribose) polymerase-1 cleavage during apoptosis: an update. *Apoptosis.* 7:321–8.
39. Wang Y, *et al.* (2011) Poly(ADP-ribose) (PAR) binding to apoptosis-inducing factor is critical for PAR polymerase-1-dependent cell death (parthanatos). *Sci. Signal.* 4:ra20.
40. Vanden Berghe T, Linkermann A, Jouan-Lanhouet S, Walczak H, Vandenabeele P. (2014) Regulated necrosis: the expanding network of non-apoptotic cell death pathways. *Nat. Rev. Mol. Cell. Biol.* 15:135–47.
41. Zhang X, *et al.* (2002) Intranuclear localization of apoptosis-inducing factor (AIF) and large scale DNA fragmentation after traumatic brain injury in rats and in neuronal cultures exposed to peroxynitrite. *J. Neurochem.* 82:181–91.
42. Komjáti K, *et al.* (2004) Poly(ADP-ribose) polymerase inhibition protect neurons and the white matter and regulates the translocation of apoptosis-inducing factor in stroke. *Int. J. Mol. Med.* 13:373–82.
43. Chen M, Zsengellér Z, Xiao CY, Szabo C. (2004) Mitochondrial-to-nuclear translocation of apoptosis-inducing factor in cardiac myocytes during oxidant stress: potential role of poly(ADP-ribose) polymerase-1. *Cardiovasc. Res.* 63:682–8.
44. Xiao CY, Chen M, Zsengellér Z, Szabo C. (2004) Poly(ADP-ribose) polymerase contributes to the development of myocardial infarction in diabetic rats and regulates the nuclear translocation of apoptosis-inducing factor. *J. Pharmacol. Exp. Ther.* 310:498–504.
45. Tóth-Zsámboki E, *et al.* (2006) Activation of poly(ADP-ribose) polymerase by myocardial ischemia and coronary reperfusion in human circulating leukocytes. *Mol. Med.* 12:221–8.
46. Callow MG, *et al.* (2011) Ubiquitin ligase RNF146 regulates tankyrase and Axin to promote Wnt signaling. *PLoS One.* 6:e22595.
47. Zhou ZD, Chan CH, Xiao ZC, Tan EK. (2011) Ring finger protein 146/Iduna is a poly(ADP-ribose) polymer binding and PARsylation dependent E3 ubiquitin ligase. *Cell Adh. Migr.* 5:463–71.
48. Wang Z, *et al.* (2012) Recognition of the iso-ADP-ribose moiety in poly(ADP-ribose) by WWE domains suggests a general mechanism for poly(ADP-ribosyl)ation-dependent ubiquitination. *Genes Dev.* 26:235–40.
49. Wang T, Simbulan-Rosenthal CM, Smulson ME, Chock PB, Yang DC. (2008) Polyubiquitylation of PARP-1 through ubiquitin K48 is modulated by activated DNA, NAD^+, and dipeptides. *J. Cell. Biochem.* 104:318–28.
50. Mashimo M, Kato J, Moss J. (2013) ADP-ribosyl-acceptor hydrolase 3 regulates poly (ADP-ribose) degradation and cell death during oxidative stress. *Proc. Natl. Acad. Sci. U. S. A.* 110:18964–9.
51. Yu X, Kem DC. (2010) Proteasome inhibition during myocardial infarction. *Cardiovasc. Res.* 85:312–20.
52. Divald A, Powell SR. (2006) Proteasome mediates removal of proteins oxidized during myocardial ischemia. *Free Radic. Biol. Med.* 40:156–64.
53. Gao Y, *et al.* (2014) Overexpression of RNF146 in non-small cell lung cancer enhances proliferation and invasion of tumors through the Wnt/β-catenin signaling pathway. *PLoS One.* 9:e85377.